Supplemental Material

Metastable State Preparation and Detection

The 404 nm laser frequency is stabilized using a Fabry-Perot cavity which is in turn stabilized to the $^1S_0 \rightarrow {}^1P_1$ laser at 399 nm, forming a transfer-lock setup, similar to the one described in [1]. The $^3D_2$ state has a linewidth of $2\pi \times 350$ kHz, with branching fractions of 0.88 and 0.12 to $^3P_1$, and $^3P_2$, respectively. Thus each ground state atom is pumped to the $^3P_2$ state after an average of $1/.12 \approx 8$ excitations. To optimize the pumping efficiency, the available 1 mW of 404 nm light is tightly focused to a waist of about 25 μm at the atomic sample and aligned along the axial direction of the ODT. Two counter-propagating laser beams are used to suppress axial dipole oscillations of the Yb* cloud due to photon recoil. The initial transfer rate is 50 Hz per atom, but the overall transfer efficiency is limited by inelastic loss. For all the experiments discussed, we remove any remaining $^1S_0$ atoms after transfer with a 3 ms light pulse resonant with the $^1S_0 \rightarrow {}^1P_1$ transition.

The transfer of Yb* to the ground state for detection is achieved by applying a 200 μs pulse of 770 nm light resonant with the $^3P_2 \rightarrow {}^3S_1$ transition. The $^3S_1$ state has a 13 ns lifetime and decays via the $^3P_1$ state to $^1S_0$. Atoms which decay to the long-lived $^3P_0$ state can be brought back into the transfer cycle with a simultaneously applied 649 nm pulse resonant with the $^3P_0 \rightarrow {}^3S_1$ transition. We typically used only the 770 nm resonant light, resulting in some atoms getting stuck in $^3P_0$. The fraction of such atoms was calibrated by comparing detection with and without the 649 nm beam and found to be 0.24(1). This is in reasonable agreement with the 0.26 value for the branching fraction obtained from the $^3S_1 \rightarrow {}^3P$ reduced matrix elements calculated in [2].

Mixture Preparation

For preparation of the Li+Yb* mixture, we begin with an initial ODT depth of $U_{\mathrm{Yb}} = 560\,\mu$K. We evaporatively cool Yb by lowering the trap depth to 15 μK in 3 s. The Yb cloud sympathetically cools an equal mixture of the two lowest hyperfine ground states of Li, which experience a 2.2 times greater optical potential at 1064 nm. We spin-purify the Li component by energetically resolving the two states (denoted $|1\rangle$ and $|2\rangle$) at a high magnetic field (480 G) and removing the upper state ($|2\rangle$) from the trap with resonant light. After preparing Yb*, we remove any remaining $^1S_0$ atoms with a 3 ms light pulse resonant with the $^1S_0 \rightarrow {}^1P_1$ transition, the last 1 ms of which is concurrent with a re-compression step where the trap depth is ramped-up to $U_{\mathrm{Yb}} = 85\,\mu$K, corresponding to a mean trap frequency of $\bar{\omega}_{\mathrm{Yb^*(Li)}} = 2\pi \times 220(1700)$ Hz. The re-compression step is done in order to suppress atom loss due to evaporation and to improve interspecies spatial overlap against differential gravitational sag. In the absence of the Yb* preparation step, the Yb-Li mixture contains $N_{\mathrm{Yb(Li)}} = 2.3(0.5) \times 10^5$ atoms at temperature $T_{\mathrm{Yb(Li)}} = 4(8)\,\mu$K. The temperature difference between the species is due to thermal decoupling at the lowest trap depths [3]. The entire experimental sequence for the mixture studies is diagrammed in Fig. S1.

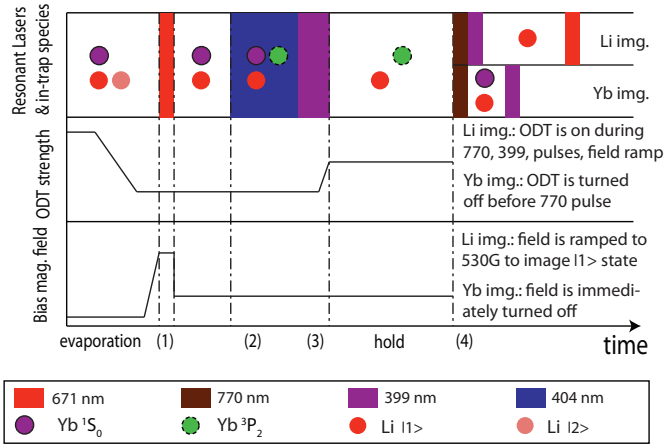

FIG. S1: (Color online). The timeline of the dual-species experiment. After evaporation, we remove the $|2\rangle$ state of lithium over 10μs with resonant light at 671 nm (1), then go to the desired magnetic field, and excite with 404 nm over 20 ms (2). Following the end of that excitation, we remove the remaining $^1S_0$ atoms in 3 ms with a resonant 399 nm pulse (3). After a variable hold time, we transfer the metastable atoms back to the ground state via $^3S_1$ and then image (4), as described.

It was important to consider the residual motion of Yb* in the ODT. The optical pumping step deposits several photon recoils of energy into the sample along the ODT axis while the differential Stark shift results in a small but instantaneous change in the trap strength. Additionally, the timescale of the re-compression step (limited by the inelastic lifetime of Yb*) is fast compared to the axial frequency of Yb* in the ODT. These often led to axial dipole oscillations of the Yb* atoms in the trap in a single 404 nm beam setup. We mitigated this effect by using two balanced counterpropagating 404 nm beams. There were still some residual damped breathing oscillations, the amplitude of which varied between different datasets. Such differences were most likely due to differences in the amount of untransferred ground state Yb atoms that can collisionally damp out these excitations, before the 399 nm removal pulse. In order to avoid this complication, we chose to analyze a data set which did not exhibit this oscillatory behavior.

Theoretical Supplement

The long-range van-der-Waals dispersion interaction is fully determined by the atomic dynamic polarizability of Li($^2S_{1/2}$) and Yb($^3P_2$) as a function of imaginary frequency [4]. The polarizability of Li is well described from the experimental data given in [5]. In the main paper, we only give details of our determination of the polarizability of the metastable Yb states.

The transition frequencies and oscillator strengths

TABLE S1: Non-relativistic and relativistic C_6 dispersion coefficients in units of $E_h a_0^6$ and magnetic dipole-dipole interaction coefficients C_3 in units of $E_h a_0^3$ between a ground-state Li and a metastable $^3P_2$ Yb atom. The non-relativistic coefficients are labeled by $^{2S+1}\Lambda$, the relativistic by $n(\Omega)$. Here, $E_h = 4.35974 \times 10^{-18}$ J is the Hartree and $a_0 = 0.0529177$ nm is the Bohr radius.

Λ	C_6	$n(\Omega)$	C_6	$C_3(10^{-5})$
$^{2,4}\Sigma$	3279.87	1(1/2)	2987.57	3.2902
$^{2,4}\Pi$	2402.98	2(1/2)	2841.42	-7.2886
		1(3/2)	2841.42	5.2091
		2(3/2)	2402.98	-9.2075
		1(5/2)	2402.97	7.9969

used in obtaining the dynamic polarizability enable us to construct both relativistic and non-relativistic van der Waals C_6 coefficients. They are listed in Table S1. The relativistic coefficients, which are directly obtained using dynamic polarizability at imaginary frequencies [6], describe the long-range interaction potentials with symmetry $n(\Omega)$, where Ω is the projection of the total electron angular momentum along the internuclear axis and n indexes states for the same Ω. For $\Omega = 1/2$, $3/2$, and $5/2$ there are 2, 2, and 1 adiabatic relativistic Born-Oppenheimer (BO) potentials dissociating to the Li($^2S_{1/2}$) + Yb($^3P_2$) limit, respectively. The non-relativistic C_6 coefficients with symmetry $^{2S+1}\Lambda$ are found from the relativistic coefficients assuming an $\vec{l}_a \cdot \vec{s}_a$ coupling between the electron orbital angular momentum $\vec{l}_a$ and spin $\vec{s}_a$ for both Li ($a = Li$) and meta-stable Yb ($a = Yb$). Our two non-relativistic coefficients differ significantly from the coefficients used in [7].

[1] S. Uetake, A. Yamaguchi, D. Hashimoto, and Y. Takahashi, Appl. Phys. B. **93**, 409 (2008).

[2] S. Porsev, Y. Rakhlina, and M. Kozlov, Phys. Rev. A **60**, 2781 (1999).

[3] V. V. Ivanov, A. Khramov, A. H. Hansen, W. H. Dowd, F. Münchow, A. O. Jamison, and S. Gupta, Phys. Rev. Lett. **106**, 153201 (2011).

[4] A. Stone, *The Theory of Intermolecular Forces*, Clarendon Press, London (1996).

[5] Y. Ralchenko, A. Kramida, J. Reader, and N. A. Team, NIST Atomic Spectra Database. Available: at http://physics.nist.gov/asd. (2011).

[6] S. Kotochigova, New J. Phys. **12**, 073041 (2010).

[7] M. Gonzalez-Martinez and J. Hutson, Phys. Rev. A **88**, 020701(R) (2013).